RSC Advances

PAPER

View Article Online
View Journal | View Issue

Cite this: *RSC Adv.*, 2016, **6**, 70501

Shape engineered TiO_2 nanoparticles in *Caenorhabditis elegans*: a Raman imaging based approach to assist tissue-specific toxicological studies†

Luca Iannarelli,[ab] Andrea Mario Giovannozzi,[a] Federica Morelli,[c] Francesco Viscotti,[c] Paolo Bigini,[c] Valter Maurino,[b] Giuseppe Spoto,[b] Gianmario Martra,[b] Erik Ortel,[d] Vasile-Dan Hodoroaba,[d] Andrea Mario Rossi*[a] and Luisa Diomede[c]

Titanium dioxide (TiO_2) nanoparticles (NPs) are one of the main sources of the nanoparticulate matter to which humans are directly exposed and several studies have demonstrated their potential toxic effects. The *in vivo* detailed spatial distribution of TiO_2 NPs is investigated herein for the first time, using a 2D chemical imaging analysis based on confocal Raman spectroscopy. The invertebrate nematode *C. elegans* was employed as a prototypical model of living organisms. Rod, bipyramidal and quasi-spherical engineered TiO_2 NPs with different primary particle sizes and agglomeration states were prepared, characterized and then administered to nematodes. Exploiting the typical fingerprint of TiO_2 in the Raman spectrum, we monitored the biodistribution of NPs inside the worm using a non-invasive, label-free method. The high spatial resolution chemical imaging and the specificity of the Raman technique in the localization of TiO_2 NPs helped in the design of behavioral *C. elegans* studies aimed at elucidating the relationship among the size, shape, and agglomeration state of NPs and their ability to induce specific toxic effects. Rod-shaped NPs were the most toxic, greatly impairing pharyngeal function, reproduction and larval growth; this indicates that the rod shape, more than the bipyramidal and spherical shapes, enables NPs to interact with biological systems. These findings indicate that this Raman-nematode combined approach represents a step forward in the field of detection of NPs in living organisms, and being rapid and inexpensive enough, it can be applied as the first screening for the ability of NPs to biodistribute and exert toxicological properties *in vivo*.

Received 14th April 2016
Accepted 12th July 2016

DOI: 10.1039/c6ra09686g

www.rsc.org/advances

Introduction

Titanium dioxide (TiO_2) is one of the most versatile metal oxide semiconductors available.[1] Its cheapness, high stability and performance mean it is widely employed in various fields, such as the environment, energy and health. Titania-based products, mostly in the form of nanoparticles (NPs), are used in applications such as dye-sensitized solar cells,[2] photocatalysis for the abatement of air and water pollutants,[3,4] and for nano-structured coatings of orthopedic and dental prostheses in the biomedical device industry.[5] Besides these applications, TiO_2 is used as a colorant additive in the European Union, where it is labeled with the code E171 (European Food Safety Authority, EFSA, 2009). With its ability to provide brightness and whiteness, TiO_2 is also employed as a pigment in personal care products, such as toothpaste and skin care lotions[6,7] and in sunscreen on account of its strong UV light-absorbing characteristics.[8] This widespread application accounts for 70% of the total production volume of pigments worldwide,[9] but the use of TiO_2 NPs is not free of adverse effects. Some toxicological studies found that they can induce cell damage, genotoxicity, inflammation and an immune response.[10] Numerous studies have indicated that TiO_2 NPs, inhaled or injected, may predispose to and/or induce carcinogenicity *in vivo* in different animal models.[11,12] On the basis of experimental evidence from animal inhalation studies, TiO_2 in nanoparticulate form was classified as a "possible carcinogen to humans" by the International Agency for Research on Cancer (IARC) and as an "occupational carcinogen" by the National Institute for Occupational Safety and Health (NIOSH).[13]

[a]*Department of Quality of Life, Food Metrology Group, INRiM, Strada delle Cacce 91, 10135, Turin, Italy. E-mail: a.rossi@inrim.it; Fax: +39 011 346384; Tel: +39 011 3919342*

[b]*Department of Chemistry, University of Turin, Via Giuria 7, 10125, Turin, Italy*

[c]*Department of Molecular Biochemistry and Pharmacology, IRCCS-Istituto di Ricerche Farmacologiche "Mario Negri", Via G. La Masa 19, 20156, Milan, Italy*

[d]*Surface Analysis and Interfacial Chemistry Division, Federal Institute for Materials Research & Testing (BAM), 12200, Berlin, Germany*

† Electronic supplementary information (ESI) available: Supporting information on dose–response test and larval growth tests are reported. See DOI: 10.1039/c6ra09686g

The rapid growth in the production and use of nanosized TiO_2, and the knowledge that NPs are chemically more reactive than bulk material due to their larger specific surface area and changed surface physicochemical properties, has greatly boosted the awareness of TiO_2 effects on consumers' health. Since 2006, numerous studies concerning the potential toxicity of TiO_2 NPs have been published.[14] *In vitro* and *in vivo* observations have indicated that TiO_2 NPs can pass through the biological membranes, entering the cells and accumulating in tissues and organs.[11] Exposure to TiO_2 NPs can cause oxidative damage, lipid peroxidation and potentially adverse effects on respiratory, cardiovascular and nervous systems.[10]

Screening of common E171 food-grade TiO_2 has shown that about 36% of the material is nanosized, with less than 100 nm in at least one dimension, indicating potentially significant dietary exposure to nano-TiO_2, especially for children.[6] These observations have led to concerns about exposure to TiO_2 NPs, especially because they are the main source of nanoparticulate matter to which humans are directly exposed.[15,16] The scientific community is consequently starting to question their potential dangers. The extent and type of the damage strongly depends on the physico-chemical features of NPs, *i.e.* size, shape, agglomeration state and chemical composition, which affect their bioavailability and reactivity. More information is needed on the response of biological systems to NPs, to elucidate and better classify their ability to biodistribute, accumulate in living organisms and cause toxicity.[17,18]

A future challenge is the application of an innovative approach employing reference nano-materials with known identity and quantity, combined with a non-invasive and label-free imaging technique to efficiently locate NPs *in vivo*. Micro (μ)-Raman imaging, using the fingerprint of TiO_2 in the Raman spectrum and the high spatial resolution for location of NPs, was applied here for the first time to investigate the detailed spatial distribution of nanoscale materials *in vivo* in a living organism, without the need for exogenous labels.

The living organism selected was the nematode *Caenorhabditis elegans*, which has well-characterized anatomical and toxicological features, allowing easy correlation between the organ-specific bio-accumulation of NPs and their biological effects. This nematode was already employed to investigate the effects of TiO_2 NPs on reproduction and development.[19] Although *C. elegans* is evolutionarily far from vertebrates, 65% of its genes have human homologues[20,21] and many human stress pathways are conserved. It is therefore a rapid and versatile system for easily recapitulating the key molecular mechanisms underlying complex toxicological features.[22] Practical reasons, including its fast reproduction, rapid growth and its transparent body,[23] were also taken into consideration.

Experimental

Materials and methods

Synthesis and preparation of TiO_2 nanoparticles (NPs) dispersions. TiO_2 rod-shaped and bipyramidal-shaped NPs were synthesized[24,25] by the forced hydrolysis of an aqueous solution of Ti^{IV}(triethanolamine)$_2$titanatrane (Ti(TEOAH)$_2$), by adding triethanolamine (TEOA) as shape controller and solid pellets of NaOH (Aldrich, ACS reagent grade) to reach the desired pH of synthesis. Bidistilled water was obtained with a Millipore MilliQ system (Millipore, Molsheim, France), with specific resistance >18.2 MΩ cm^{-1} and TOC <5 ppb. Ti(TEOAH)$_2$titanatrane, obtained from the reaction between TEOHA (Aldrich, reagent grade 98%) and Ti(IV) isopropoxide (Aldrich, reagent grade 98%), was filtered with a 0.45 μm cellulose acetate membrane filter and N_2 sparged in a Teflon-lined stainless steel reactor, before sealing it. The reactor was heated to 40 °C, then to the temperature desired for the treatment at 1 °C min^{-1}; the temperature was kept for the scheduled time. The reactor was then cooled in air. Different synthesis conditions provided rod-like anatase NPs (SNM1) and truncated bipyramidal anatase NPs (SNM2). A temperature of 140 °C and a pH ≈ 11 were used to prepare SNM1, while 220 °C and a pH ≈ 10 were set to obtain SNM2. SNM3 NPs (agglomerated form of truncated bipyramidal nanoparticles) were prepared starting from the SNM2 sample that was initially dried using a work-up procedure, in order to obtain the nanopowder. The work-up of the synthesized NPs suspensions involved the following steps: dialysis (against ultrapure water, using Spectra/Por dialysis membrane tubing MWCO 8–14 kDa), irradiation (after the addition of 50 g l^{-1} H_2O_2, under UV light using a Medium Pressure Mercury Lamp), dialysis and freeze-drying. SNM3 dispersions were prepared using an ultrasonication treatment to obtain stable and controlled agglomerated suspensions. Powders of TiO_2 NPs were dispersed in a water solution containing 9% of TEOA at the final concentration of 1 g l^{-1}. Ultrasonication consists of three steps: (a) 20 min in 80 W ultrasonic bath at 15 °C, continuum mode; (b) 60 min in 360 W ultrasonic bath at 15 °C, pulse mode (1 Hz); (c) 20 min in 80 W ultrasonic bath at 15 °C, continuum mode. After sonication, dispersions were filtered with nylon membrane hydrophilic filters (0.45 μm porous) and stored at room temperature.

Quasi-spherical commercial titanium(IV) oxide anatase NPs, <25 nm in size, were purchased from Sigma Aldrich (Sigma). Dispersions of Sigma NPs were prepared following the same ultrasonication procedure for SNM3, as described above.

Transmission-scanning electron microscopy (T-SEM). The dimensional characterization (size and shape) of TiO_2 NPs was done with SEM using a Zeiss Supra 40 instrument (Zeiss, Oberkochen, Germany) equipped with a Schottky field emitter and the standard Everhart-Thornley detector with high-resolution (InLens detector). The surface-sensitive InLens SEM mode and T-SEM suited for dimensional measurements were applied to the same field of view on the sample. More details on this method and instrumental approach, with advantages and disadvantages, have already been reported.[26–28]

Dynamic laser scattering (DLS) analysis. DLS measurements were made using a Delsa Nano™ C Analyzer (Beckman Coulter) equipped with a 638 nm diode laser and a temperature control. The laser fluctuation was detected on a photomultiplier tube detector positioned behind the cuvette with an angle of 163°. Hydrodynamic diameters were calculated, setting the temperature at 25 °C, viscosity (η) 0.890 cP and refractive index of water 1.3325. Dispersion stability was monitored for four days.

Raman spectroscopy analysis. Raman spectroscopy analyses on TiO_2 NPs powders were conducted with a DXR™ Raman Microscope (Thermo Scientific) using a laser wavelength of 532 nm, laser power of 1 mW and a 20× long working distance microscope objective. Spectra were collected in the 50–1800 cm^{-1} spectral region, with a grating resolution of 3.3–3.9 cm^{-1}, exposure time of 1 s and 20 scans in total.

Micro (μ)-Raman imaging spectroscopy. μ-Raman imaging spectroscopy of *C. elegans* was conducted 24 h after administration of TiO_2 NPs with a DXR™xi Raman Imaging Microscope (Thermo Scientific) using a laser wavelength of 532 nm, laser power 5 mW, a 50× microscope objective and a motorized stage with a 2 μm step. Spectra were collected in the 50–3500 cm^{-1} spectral region with a grating resolution of 5 cm^{-1}, exposure time of 0.025 s and 50 scans in total. The Raman chemical image was presented using a color scale from blue to red, indicating the absolute intensity of the typical E_g band of anatase TiO_2 at 143 cm^{-1}. Confocal Raman imaging depth profiling was also conducted in the area of TiO_2 NPs agglomerates using a 2 μm offset. Spectra collection and chemical image representation were the same as the above cited measurements.

***C. elegans* experiments.** Bristol N_2 strain from the *Caenorhabditis elegans* Genetic Center (CGC; University of Minnesota) was propagated at 20 °C on solid Nematode Growth Medium (NGM) seeded with *Escherichia coli* OP50 (from CGC) for food. To prepare age-synchronized animals, nematodes were transferred to fresh NGM plates on reaching maturity at three days of age and allowed to lay eggs overnight. Isolated hatchlings from the synchronized eggs (day 1) were cultured on fresh NGM plates at 20 °C. Nematodes (L3–L4 larval stage) were collected with M9 buffer, centrifuged and washed twice with 5 mM phosphate buffered saline (PBS), pH 7.4, to eliminate bacteria. Nematodes were resuspended in distilled water (100 worms per 100 μl) and were fed for 2 h with 0.01–1 mg l^{-1} of TiO_2 NPs in distilled water (SNM1, SNM2, SNM3 and Sigma) in the absence of *E. coli* to avoid any potential interference between bacteria and NPs. Control worms were fed the same volume of distilled water (vehicle) only. After 2 h of orbital shaking, the worms were then transferred onto NGM plates seeded with fresh OP50 *E. coli*. The effect of TiO_2 NPs on the pharyngeal pumping rate of worms was scored from 2 h up to 24 h later by counting the number of times the terminal bulb of the pharynx contracted over a 1 minute interval (pumps per min).[29] To determine the effect of NPs on egg laying and larval growth, worms fed for 2 h with 0.2 mg l^{-1} of SNM1, SNM2, SNM3 and Sigma as described above, were singularly transferred onto NGM plates seeded with fresh OP50 *E. coli* and allowed to lay eggs for 18 h at 20 °C. Adults were then removed and the number of the eggs laid was scored. The larval growth was then followed by counting the number of worms at L1/L2, L2/L3 and L4/adult larval stage, respectively, at 13 h, 22 h and 40 h after.[30]

Statistical analysis. The data were analyzed using GraphPad Prism 4.0 software by an independent Student's *t* test and one-way analysis of variance (ANOVA) and Bonferroni *post hoc* analysis. Vehicle and NPs effects were compared using an independent Student's *t* test and the 50% inhibition/inhibitory concentration (IC_{50}) was determined using Prism version 4.0 for Windows (GraphPad Software). A p value < 0.05 was considered significant.

Results and discussion

In order to establish a relationship among the physico-chemical features of NPs and their ability to accumulate in specific tissues, inducing a toxic effect, well-defined controlled protocols for the production of engineered anatase TiO_2 NPs with different sizes, shapes and agglomeration states were employed.[31] We fabricated engineered rod-shaped TiO_2 NPs (SNM1) and two types of engineered TiO_2 NPs of the same size and bipyramidal shape, but a different agglomeration state in solution (SNM2 and SNM3). Commercial quasi-spherical titanium(IV) oxide NPs (Sigma Aldrich) were tested for comparison. NPs were morphologically characterized with a Field Emission (FE)-Scanning Electron Microscope (SEM) equipped with a transmission-unit (T-SEM).

SNM1 rod-shaped TiO_2 NPs were 108 ± 47 nm long with an aspect ratio of approximately 1 : 5 (Fig. 1). The two bipyramidal TiO_2 NPs SNM2 and SNM3 were produced following the same experimental protocol, and had the same primary particle size

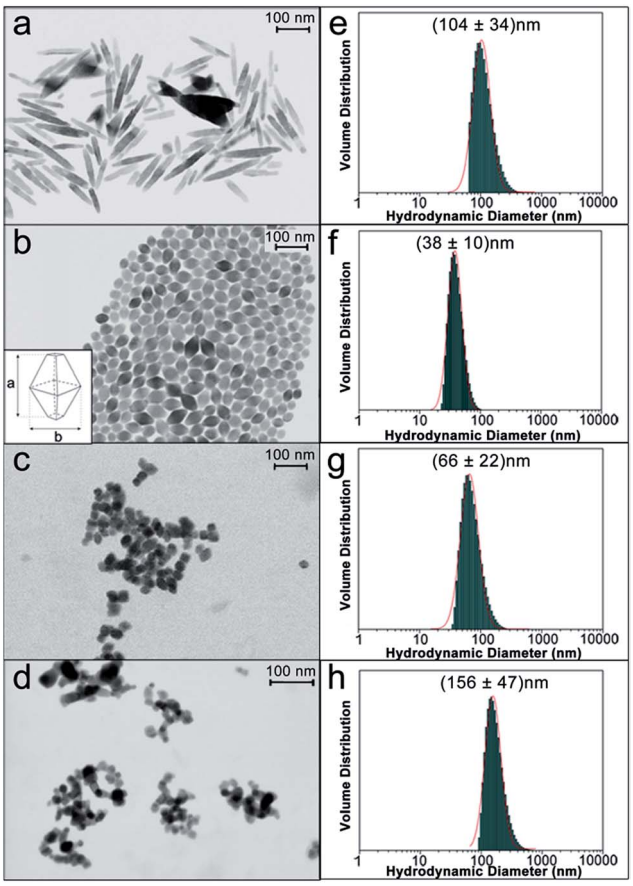

Fig. 1 (a–d) SEM micrographs of rod-shaped SNM1 (a), bipyramidal SNM2 (b) and SNM3 (c), and commercial Sigma (d) TiO_2 NPs. (e–h) DLS analyses, normalized by volume distribution of SNM1 (e), SNM2 (f), SNM3 (g) and Sigma commercial (h) NP suspensions.

of 50 ± 9 nm, as measured by SEM analysis, with an aspect ratio of 3 : 2. The size was calculated on the long axis of the bipyramid, indicated in Fig. 1b.

SNM2 NPs were used after the hydrothermal synthesis, while SNM3 NPs were dried under vacuum then dispersed in water by ultrasonication (see Materials and methods) to generate a bigger agglomeration state. Fig. 1c shows a representative SEM image taken on a more diluted dispersion of a SNM3 NPs sample in order to observe suspended agglomerates better and prevent large-scale coalescence. Commercial TiO_2 NPs (Fig. 1d) had a wider size distribution with particles ranging from 10 nm up to 30 nm, and the mean value at 19 ± 6 nm. These NPs were quasi-spherical (Fig. 1d).

Aqueous dispersions of TiO_2 NPs were also characterized by Dynamic Light Scattering (DLS) as a quick method for sizing and determining their state of agglomeration in suspensions and their stability. Size distributions of engineered TiO_2 NPs were mono-modal and narrow by DLS analysis, with hydrodynamic diameters of 104 ± 34 nm, 38 ± 10 nm and 66 ± 22 nm for SNM1, SNM2 and SNM3, respectively (Fig. 1e–g). The results of DLS and SEM analysis clearly show that SNM3 NPs had a mean hydrodynamic diameter of 66 nm, which was almost twice its primary particle size (38 nm), proving that agglomeration occurred in solution.

DLS measurements for SNM1 and SNM2 NPs (Fig. 1e and f) were in accordance with the primary particle size measured on the long axis by SEM (Fig. 1a and b), meaning that no agglomeration occurred in solution. DLS analyses on the engineered NPs were repeated over a period of 24 hours to prove the stability of the suspensions: no significant changes in size were detected after 96 hours (Fig. S1†). A spread, bimodal distribution of the hydrodynamic diameter was observed for commercial TiO_2 NPs (Fig. 1h). There were big agglomerates in solution with the most abundant population centered at 156 nm hydrodynamic diameter. NPs characterization by DLS provided valuable information on their actual size when suspended in solutions. As these formulations were then to be administered to *C. elegans*, DLS data were considered fundamental to correlate the size of NPs with their *in vivo* effects.

To examine the crystalline composition of the TiO_2 NPs, Raman spectroscopy was done. As previously demonstrated by X-ray diffraction (XRD),[24] all the NPs we employed were in the anatase phase. A typical fingerprint of the anatase TiO_2 is shown in the Raman spectra in Fig. 2, with the characteristic phonon active bands E_g at 143 cm^{-1}, E_g at 197 cm^{-1}, A_{1g} at 397 cm^{-1}, B_{1g} at 515 cm^{-1} and E_g at 639 cm^{-1} for all the NPs.[32] Since the E_g band at 143 cm^{-1} is the most intense in the molecular fingerprint of the anatase TiO_2, and the region between 50 and 400 cm^{-1} in the Raman spectrum is usually free of the vibrational bands of biological tissues,[33,34] this signal was selected to sensitively locate the TiO_2 NPs inside the body of *C. elegans*.

Nematodes were fed with 0.2 μg ml^{-1} of TiO_2 NPs: this dose level is well below the lethal dose and about five hundred times lower than that reported to be toxic for worms.[35] Twenty-four hours after the administration of TiO_2 NPs, single specimens of *C. elegans* were laid on a CaF_2 Raman grade window and analyzed by Raman spectroscopy. A fast Raman imaging system

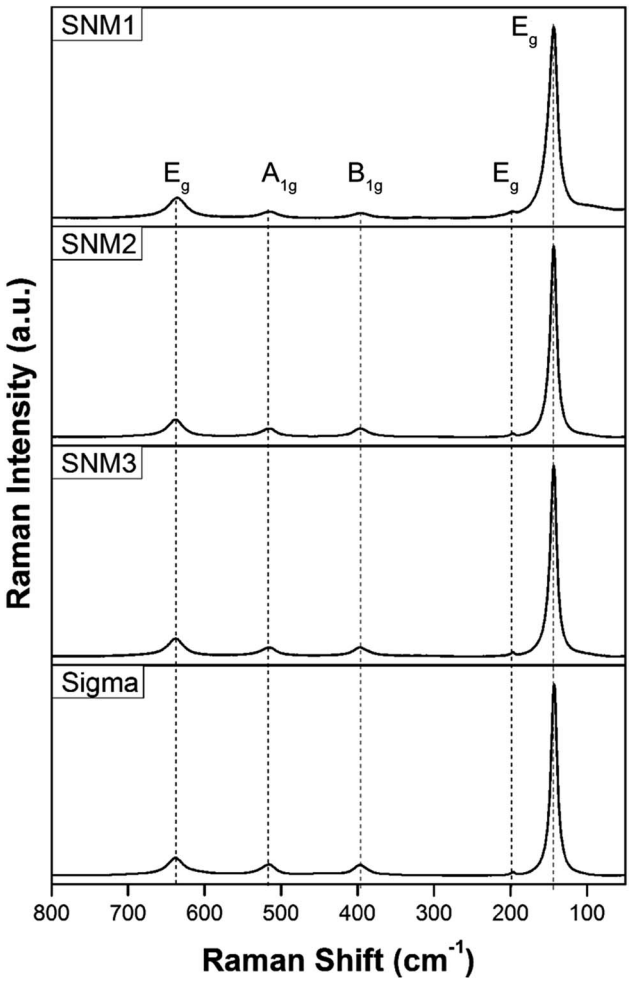

Fig. 2 Raman spectra and related peak assignment of rod-shaped SNM1, bipyramidal SNM2 and SNM3, and commercial Sigma TiO_2 NPs.

equipped with a 50× microscope objective and a motorized stage with 2 μm step size was used to examine the distribution of the NPs inside the body.

A representative Raman mapping performed on a whole *C. elegans* fed with commercial TiO_2 NPs is illustrated in Fig. 3. The contrast phase image of the worm was overlaid with the Raman map from the distribution profile of the E_g band intensity at 143 cm^{-1} over the area analyzed (Fig. 3a) and a color scale bar from blue to red was used to illustrate the intensity of the anatase E_g band, providing semi-quantitative information of the TiO_2 NP localization.

Several independent experiments were performed, analyzing nematodes fed NPs with different shapes, and as indicated by the representative Raman mapping performed on worms fed Sigma NPs (Fig. 3a), as well as the other types of NPs (Fig. 4–6), we observed that TiO_2 mainly localized in two regions of the worm's body. Selective magnification of these regions allowed more specific location of TiO_2 NPs. Which accumulated as agglomerates in the pharynx (Fig. 3b) and around the vulval region (Fig. 3c). A Raman spectrum in these regions (Fig. 3d) showed an intense band at 143 cm^{-1} corresponding to a characteristic TiO_2 anatase structure, while other signals, in the

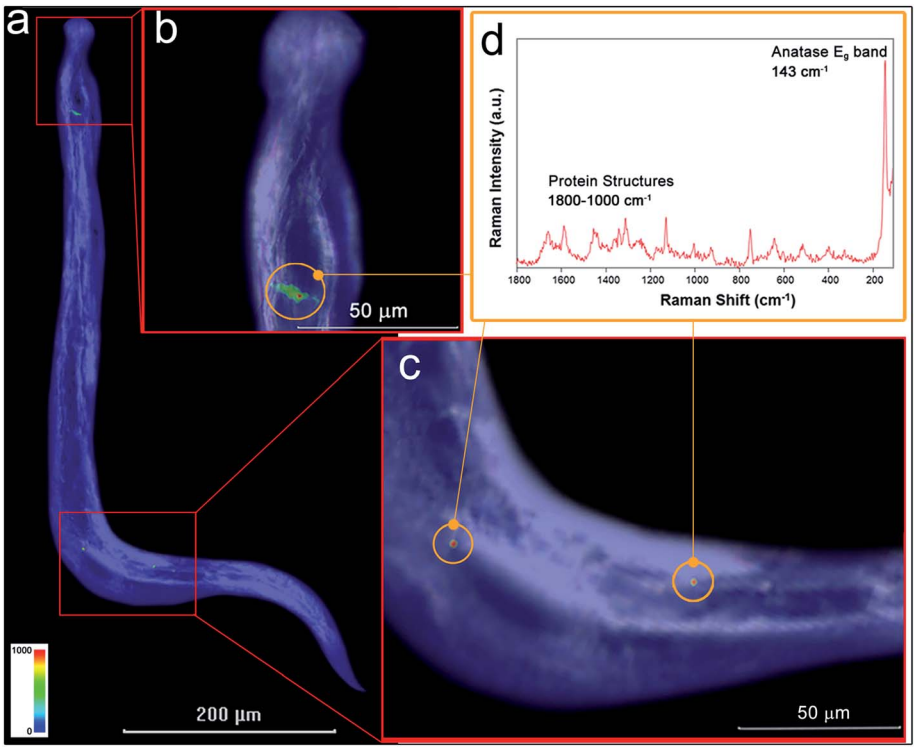

Fig. 3 Raman mapping on *C. elegans* fed with 0.2 μg ml^{-1} commercial Sigma TiO_2 NPs for 24 h. Contrast phase image of the worm overlaid with a Raman map obtained from monitoring the E_g band intensity at 143 cm^{-1} over the area analyzed. A color scale from blue to red was used to visualize the intensity of the anatase E_g band (a). Orange circles show the magnification of the pharyngeal (b) and vulval (c) regions of the worm, showing TiO_2 NPs agglomerates. Raman spectrum collected on TiO_2 NPs agglomerate shows the anatase E_g band at 143 cm^{-1} and protein structures of worm tissues in the range 1800–1000 cm^{-1} (d).

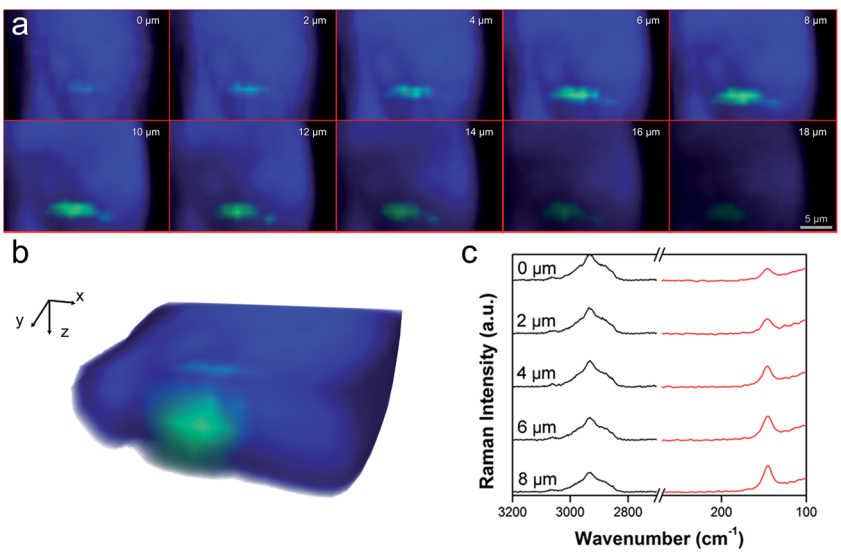

Fig. 4 (a) Confocal Raman depth profile mapping in the pharynx region of *C. elegans* fed with 0.2 μg ml^{-1} of commercial Sigma TiO_2 NPs for 24 h. Color maps at different depth profiles (0–18 μm) were made by the sum of the green chemical image, related to the height of the E_g mode of anatase TiO_2 at 143 cm^{-1}, and the blue chemical image, related to the height of the CH_2 signal at 2920 cm^{-1}, specific to worm tissue; (b) 3D reconstruction of a cross-section of the worm showing the TiO_2 NPs agglomerate. (c) Raman spectra collected in the region of the TiO_2 NP agglomerate from 0 to 8 μm of depth, showing the increased intensity of TiO_2 E_g mode at 143 cm^{-1} at deeper penetration.

1000–1800 cm^{-1} spectral region, can be ascribed to the amide signals of the protein structures composing the nematode's tissues.[33,34]

To demonstrate that TiO_2 NPs were really inside the worm's organs and not only deposited on its body surface, confocal Raman depth profiles were also recorded (Fig. 4). Color maps at

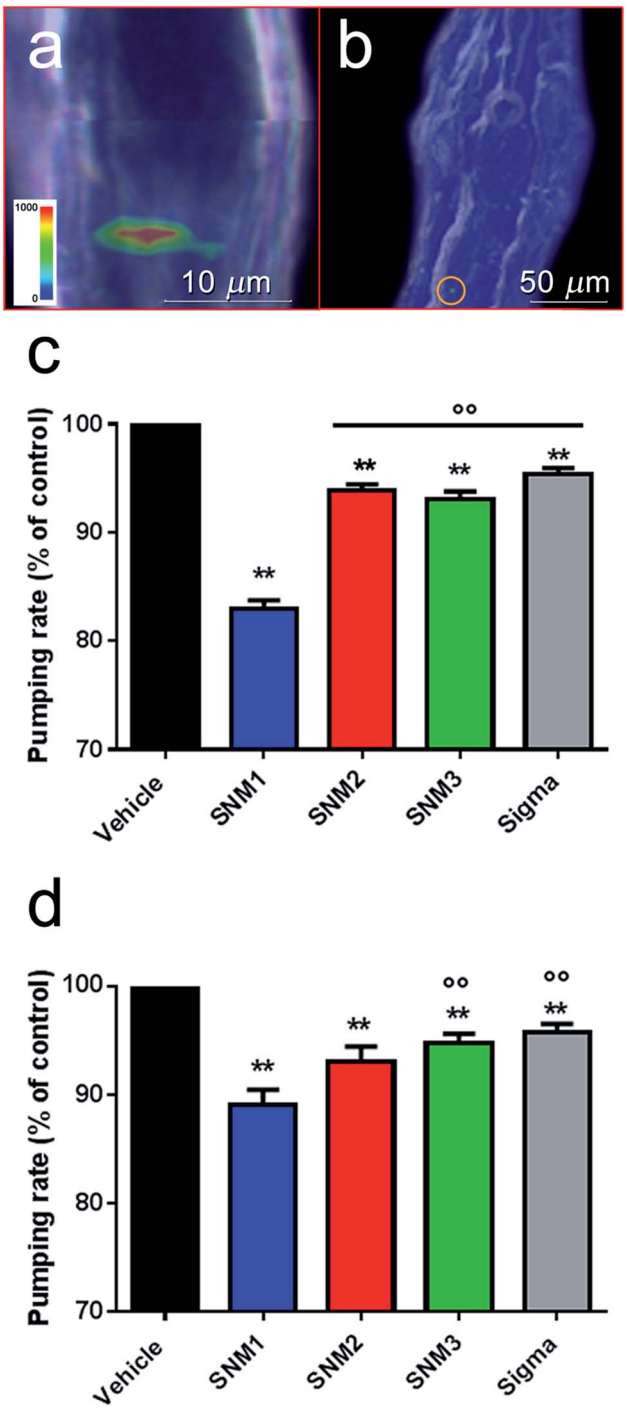

Fig. 5 Raman mapping in the pharyngeal area of *C. elegans* fed with 0.2 μg ml^{-1} of commercial Sigma TiO_2 NPs (a) and 0.2 μg ml^{-1} of SNM2 (b) for 24 h. Color scale bars illustrate the intensity of the characteristic E_g anatase band at 143 cm^{-1}. (c and d) The effect of NPs on pharyngeal function. Nematodes (100 worms per 100 μl) were fed for 2 h with 0.2 μg ml^{-1} of different NPs (Sigma, SNM1, SNM2 or SNM3) suspended in distilled water in the absence of OP50 *E. coli* and then plated on Nematode Growth Medium (NGM) plates seeded with the bacteria. Control worms were fed distilled water alone (vehicle). Pharyngeal pumping was scored (c) 2 h and (d) 24 h after plating. Data are expressed as the mean ± standard error (SE) (40 worms per group). $^{**}p < 0.01$ *vs.* vehicle and $^{\circ\circ}$ $p < 0.01$ *vs.* SNM1, according to one-way ANOVA and Bonferroni *post hoc* test.

different depth profiles (0–18 μm) were made by the superimposition of the green chemical image, related to the height of the E_g mode of anatase TiO_2 at 143 cm^{-1}, and the blue chemical image, related to the height of the CH_2 signal at 2920 cm^{-1}, specific to worm tissue (Fig. 4a). A 3D reconstruction of the cross-section of the worm (Fig. 4b), obtained by the sum of the Raman depth profile images in Fig. 4a, shows the internalization of TiO_2 NPs inside the body of the worm. Raman spectra in the region of the TiO_2 NPs agglomerate show the increased intensity of the TiO_2 E_g mode at 143 cm^{-1} at deeper penetration, while the CH_2 signal at 2920 cm^{-1} keeps the same intensity from 0 μm to 8 μm of depth (Fig. 4c). These results clearly indicate that TiO_2 NPs once ingested, can pass the biological membranes of the pharyngeal channel and accumulate in the tissue of the terminal bulb. TiO_2 located similarly in worms fed with all the types of NP considered here (Fig. 3–6), suggesting that their primary size, shape and agglomeration state did not affect their ability to accumulate in the nematode organs. However, since the Raman method applied here provides semi-quantitative information, definitive conclusions on whether the shape of NPs can affect the amount of TiO_2 accumulated in the organs cannot be drawn. We then investigated whether the tissue-specific accumulation of TiO_2 NPs in nematodes resulted in changes to their physiological functions. Behavioral tests were run on *C. elegans* from 2 hours up to 24 hours after feeding with the different TiO_2 NPs. In view of the accumulation of TiO_2 NPs in the pharynx (Fig. 5a and b), pharyngeal function was evaluated by scoring the "pumping rate", *i.e.* the number of times the terminal bulb of the pharynx contracted in one minute.[29] Two hours after feeding, a 17% impairment of pharyngeal function was seen in worms fed SNM1 and a smaller but significant decrease was observed in nematodes fed with the other TiO_2 NPs (Fig. 5c). Comparable inhibition of pharyngeal function was still present 24 hours after feeding, indicating that these NPs can cause a permanent functional damage (Fig. 5d). At each time point, the pharyngeal impairment was more pronounced in worms fed SNM1 than in those fed the other NPs. This was supported by comparison of the 50% inhibitory concentrations (IC_{50}) obtained from the dose–response curves (Fig. S2†).

TiO_2 NPs were also found in the worms' reproductive system and a deeper Raman imaging study close to the area indicated that NPs can accumulate in the vulval region and inside eggs (Fig. 6a–c) through transition from the intestine. Experimental evidence in vertebrates has shown that TiO_2 NPs can pass the placenta, reaching fetal tissues, and previous studies in nematodes indicated that they may cause reproductive and developmental defects, and malformations.[10]

In order to see whether the localization of the different TiO_2 NPs in these regions can result in dysfunctions in the adult worms' ability to reproduce, we studied the number of eggs laid (Fig. 6d). SNM1 and SNM2 NPs significantly affected the worms' ability to reproduce, the number of eggs laid being reduced by 73% and 43%, respectively. A small, although not significant reduction was observed in worms fed SNM3, while Sigma NPs had no effect (Fig. 6d).

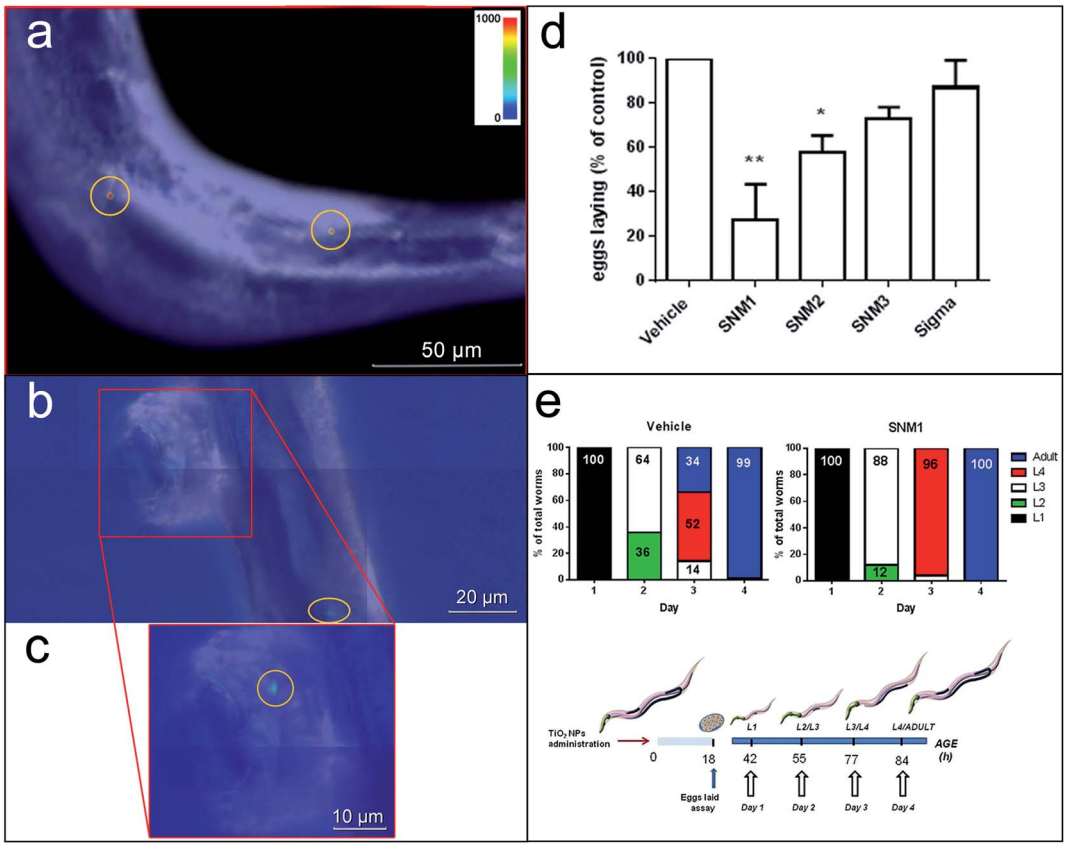

Fig. 6 Raman mapping in the vulval region (a and b) and inside an egg (c) of *C. elegans* fed with 0.2 μg ml^{-1} commercial Sigma TiO_2 NPs or 0.2 μg ml^{-1} of SNM3 for 24 h. Color scale bars illustrate the intensity of the characteristic E_g anatase band at 143 cm^{-1}. (d and e) Effect of NPs on egg laying and larval growth. Nematodes at L4 larval stage (100 worms per 100 μl) fed for 2 h with 0.2 μg ml^{-1} of the different types of NP suspended in distilled water (Sigma, SNM1, SNM2 or SNM3) in the absence of OP50 *E. coli* were then plated on NGM plates seeded with bacteria. Control worms were fed distilled water alone (vehicle). (d) The number of eggs laid 18 h after plating was scored and expressed as a percentage of the eggs laid by vehicle-fed worms. Mean ± standard error (SE) (10 worms per group). *$p < 0.05$ and **$p < 0.01$ *vs.* vehicle, according to the one-way ANOVA and Bonferroni *post hoc* tests. (e) L1 larval stage nematodes (100 per plate), from eggs laid by worms fed NPs were plated onto fresh NGM plates seeded with OP50 for food (day 1). Larval growth was rated, scoring 13, 22, 40 and 66 h after plating, counting worms at L2, L3, L4 and adult stages, on days 2, 3 and 4. Data are expressed as percentage of the total worms. Diagram of the assays in worms, showing when the TiO_2 NPs were administered and when the eggs laid and larval growth assays were performed.

These results suggest that the reduction of the number of eggs is strongly influenced by the size of the NPs and also by their agglomeration state. The agglomerates impaired the reproduction less than the monodisperse preparations, as clearly shown with bipyramidal SNM2 and SNM3 preparations, and with the highly agglomerated Sigma NPs. For SNM1 NPs, the rod-shape is probably more effective than size in reducing the eggs laid.

Since SNM1 NPs significantly impaired reproduction, we also investigated the effect on the development of larvae (Fig. 6e). SNM1 rod NPs significantly modified the different stages of the development of larvae (L1, L2, L3, L4 and adult). They seemed to increase the speed of larval growth. At day 2 of age, there was a smaller percentage of worms in L2 and a higher percentage in L3, compared to worms fed vehicle. This resulted in a much larger percentage of worms in L4 at day 3: 96% compared to 52% of vehicle-fed nematodes (Fig. 6e). There were only minimal or no significant effects on the development of larvae from worms fed SNM2, SNM3 and Sigma NPs (Fig. S3†). It cannot be excluded that the effect of SNM1 on the acceleration of the development in the progeny may be related to the adaptive response of worms against a toxicant, in order to accelerate their reproduction, keeping the species alive.[36]

Food-grade E171 TiO_2, commonly used as additive in food and personal care products, was described as containing NPs with polyhedric shapes and a very broad size distribution, ranging from 30 to 400 nm.[6] Based on our observation that the size and shape of TiO_2 NPs did not affect their biodistribution, we can expect that E171 will be accumulated in *C. elegans*, similarly to the NPs considered in this study. Being that the physical and chemical properties of E171 are different from those of the NPs tested here, it is difficult to predict its toxicity effect.

Conclusions

Our findings indicate that confocal μ-Raman spectroscopy is a non-invasive, label-free technique for examining the

distribution of TiO_2 nanomaterials in a whole living organism, with a high spatial resolution chemical imaging method. This enabled us to plan tissue-specific toxicological studies to see how NPs affected important physiological functions. It is also important to use nanosized reference materials with known identity and quantity to establish the relationships between the size, shape and agglomeration state of NPs, and their ability to biodistribute, pass through biological membranes, accumulate in specific tissues, and exert a toxic effect.

The toxicological data presented indicate that the size and shape of TiO_2 NPs did not affect their ability to biodistribute and accumulate in *C. elegans*, but strongly influenced their toxicity. All the TiO_2 NPs ingested were able to pass the intestinal barrier and reach the worms' reproductive apparatus, as indicated by the effects on egg deposition and larval development. SNM1 NPs had the greatest effect on pharyngeal function, reproduction and larval growth, indicating that the rod shape, more than the bipyramidal and spherical shapes, enabled NPs to interact with biological systems. The impairment of reproduction mainly depends on the size of the TiO_2 NPs and on their agglomeration state, agglomerates being less effective than the monodisperse preparations in reducing the number of eggs laid, as indicated by the bipyramidal SNM2 and SNM3 preparations, and the high-agglomerated Sigma NPs. No correlation was observed with the size and agglomeration state in the impairment of pharyngeal motility, where SNM2, SNM3 and Sigma NPs caused comparable inhibition, with permanent functional damage. This combined Raman-nematode approach is rapid and inexpensive enough to be applied as the first screening for the ability of NPs to biodistribute and exert toxicological properties *in vivo*. In line with the three Rs guiding principles on the humane use of animals in scientific research, this alternative approach also offers the advantage of avoiding ethical issues involving the use of vertebrates, and by guiding the design of tissue-specific toxicological evaluation, it helps to minimize the number of animals needed.

Acknowledgements

This work was supported by the SETNanoMetro Seventh Framework Programme project (project number 604577; call identifier FP7-NMP-2013_LARGE-7). *C. elegans* strains and *E. coli* OP50 were provided by CGC, which is funded by NIH Office of Research Infrastructure Program (P40 OD010440).

References

1 X. Chen and S. Mao, *Chem. Rev.*, 2007, **107**, 2891.
2 M. J. Grätzel, *J. Photochem. Photobiol., C*, 2003, **4**, 145.
3 K. Nakata and A. J. Fujishima, *J. Photochem. Photobiol., C*, 2012, **13**, 169.
4 M. A. Lazar, S. Varghese and S. S. Nair, *Catalysts*, 2012, **2**, 572.
5 L. G. Gutwein and T. J. Webster, *Biomaterials*, 2004, **25**, 4175.
6 A. Weir, P. Westerhoff, L. Fabricius and N. von Goetz, *Environ. Sci. Technol.*, 2012, **46**, 2242.
7 Y. Yang, K. Doudrick, X. Bi, K. Hristovski, P. Herckes, P. Westerhoff and R. Kaegi, *Environ. Sci. Technol.*, 2014, **11**, 6391.
8 N. Serpone, D. Dondi and A. Albini, *Inorg. Chim. Acta*, 2007, **360**, 794.
9 K. H. Buchel, H. H. Moretto and P. Woditsh, *Industrial Inorganic Chemistry*, Wiley-VCH, Winheim, 2000, p. 553.
10 H. Shi, R. Magaye, V. Castranova and J. Zhao, *Part. Fibre Toxicol.*, 2013, **10**, 15.
11 H. Christie, R. J. Mackay and A. M. Fisher, *Am. Ind. Hyg. Assoc*, Taylor & Francis Group, 1963.
12 K. P. Lee, H. J. Trochimowicz and C. F. Reinhardt, *Toxicol. Appl. Pharmacol.*, 1985, **79**, 179.
13 IARC, Working Group on the Evaluation of Carcinogenic Risks to Humans, *IARC monographs on the evaluation of carcinogenic risks to humans*, 2010, p. 93.
14 K. Juganson, A. Ivask, I. Blinova, M. Mortimer and A. Kahru, *Beilstein J. Nanotechnol.*, 2015, **6**, 1788.
15 C. Contado, *Front. Chem.*, 2015, **3**, 1.
16 M. I. Setyawati, C. Y. Tay and D. T. Leong, *Small*, 2015, **11**, 3458.
17 N. Shinohara, N. Danno, T. Ichinose, T. Sasaki, H. Fukui, K. Honda and M. Gamo, *Nanotoxicology*, 2014, **8**, 132.
18 T. P. J. Linsinger, Q. Chaudhry, V. Dehalu, P. Delahaut, A. Dudkiewicz, R. Grombe, F. von der Kammer, E. H. Larsen, S. Legros, K. Löschner, R. Peters, R. Ramsch, G. Roebben, K. Tiede and S. Weigel, *Food Chem.*, 2013, **138**, 1956.
19 B. Song, J. Liu, X. Feng, L. Wei and L. Shao, *Nanoscale Res. Lett.*, 2015, **10**, 1042.
20 R. Koeber, T. P. J. Linsinger and H. Emons, *Accredit. Qual. Assur.*, 2010, **15**, 255.
21 E. Culetto and D. B. Sattelle, *Hum. Mol. Genet.*, 2000, **9**, 869.
22 S. Brenner, *Genetics*, 1974, **77**, 71.
23 M. Corsi, A. K. Wightman and B. Chalfie, *Genetics*, 2015, **200**, 387.
24 C. Deiana, M. Minella, G. Tabacchi, V. Maurino, E. Fois and G. Martra, *Phys. Chem. Chem. Phys.*, 2013, **15**, 307.
25 F. Pellegrino, L. Pellutiè, C. Deiana, G. Martra, E. Ortel, V. D. Hodoroaba, D. Taloi, R. Isopescu, D. Imbraguglio, A. M. Rossi and V. Maurino, Design rules for the Hydrothermal Synthesis of Shape and Size Controlled Anatase Nanoparticles, Manuscript in preparation.
26 P.-J. De Temmerman, E. Verleysen, J. Lammertyn and J. Mast, *Powder Technol.*, 2014, **261**, 191.
27 V.-D. Hodoroaba, C. Motzkus, T. Macé and S. Vaslin-Reimann, *Microsc. Microanal.*, 2014, **20**, 602.
28 V.-D. Hodoroaba, D. Akcakayiran, D. O. Grigoriev and D. G. Shchukin, *Analyst*, 2014, **139**, 2004.
29 L. Diomede, P. Rognoni, F. Lavatelli, M. Romeo, E. Del Favero, L. Cantù, E. Ghibaudi, A. Di Fonzo, A. Corbelli, F. Fiordaliso, G. Palladini, V. Valentini, V. Perfetti, M. Salmona and G. Merlini, *Blood*, 2014, **123**, 3543.
30 L. Diomede, C. Soria, M. Romeo, S. Giorgetti, L. Marchese, P. P. Mangione, R. Porcari, I. Zorzoli, M. Salmona, V. Bellotti and M. Stoppini, *PLoS One*, 2012, **7**(12), e52314.
31 http://www.setnanometro.eu/.

32 H. C. Choi, Y. M. Jung and S. B. Kim, *Vib. Spectrosc.*, 2005, **37**, 33.
33 Z. Movasaghi, S. Rehman and I. Rehman, *Appl. Spectrosc.*, 2007, **42**, 493.
34 A. Rygula, K. Majzner, K. M. Marzec, A. Kaczor, M. Pilarczyk and M. Baranska, *J. Raman Spectrosc.*, 2013, **44**, 1061.
35 H. Wang, R. L. Wick and B. Xing, *Environ. Pollut.*, 2009, **157**, 117.
36 L. Zhang, D. G. Gualberto, X. Guo, P. Correa, C. Jee and L. R. Garcia, *Nat. Commun.*, 2015, **6**, 6345.